Stress intensity factor solutions for several crack problems using the proportional crack opening displacements

著者	Lan Xin, Ji Shaobo, Noda Nao-Aki, Cheng Yong
journal or publication title	Engineering fracture mechanics
volume	171
page range	35-49
year	2016-12-24
URL	http://hdl.handle.net/10228/00007022

doi: info:doi/10.1016/j.engfracmech.2016.12.002

Stress intensity factor solutions for several crack problems using the proportional crack opening displacements

Xin Lan[1], Shaobo Ji[1], Nao-Aki Noda[2], Yong Cheng[1]
1. School of Energy and Power Engineering, Shandong University, Jingshi Road 17923#, Jinan, Shandong province, China
2. Department of Mechanical Engineering, Kyushu Institute of Technology,1-1 Sensui- cho, Tobata-ku, Kitakyushu-shi, Fukuoka, 804-8550, Japan

XinLan
School of Energy and Power Engineering
Shandong University
Jingshi Road 17923#, Jinan, Shandong province, China
lanxin@sdu.edu.cn
Tel: (+86)-15969685185

ABSTRACT

A general finite element procedure based on the proportional crack opening displacements for obtaining the stress intensity factors is presented. The procedure is applied to the nonsingular 3-node linear, 4-node linear, 8-node parabolic, 8-node axisymmetric elements and 8-node hexahedral solid elements for a test. It is found that the current method exhibits good element type adaptability and significantly less mesh dependency, and accurate results can be obtained effectively using rather coarse meshes. The accuracy of the current procedure is evaluated by applying it to two-dimensional interface cracks, three-dimensional penny-shaped cracks as well as circumferential surface cracks. Comparison with the published data from the literature shows that the current procedure gives accurate stress intensity factors. Furthermore, the current method is fairly efficient and less computational resource consuming and can be used as an effective tool in the reliability analysis of the bonded multi-layers.

Keywords： Stress intensity factor; Crack opening displacement; Interfacial crack; Finite element method

1. Introduction

Bi-material interfaces are widely observed in the modern composite structures. The presence of an interface crack may eventually cause a through thickness crack which results in the final failure of a structure. The singular stress field around an interface crack was firstly discovered by Williams [1], then his work was followed and extended by Rice and Sih [2], Erdogan [3,4], England[5], Willis [6] and many others. Following their pioneering research, a variety of algorithms have been developed based on LEFM and in conjunction with the analytical method or the numerical method. The analytical methods for solving the stress intensity factors (SIFs) for the interfacial crack problems are only limited to a few specific cases due to the inherent mathematical difficulties. Therefore, general numerical methods are necessary to be employed to treat the more general cracked bodies in the practical applications. In this paper, a brief summary regarding the numerical methods available for computing the SIFs of the interface cracks using FE analysis will be reviewed and discussed. Then, a finite element procedure using the proportional relative crack opening displacement (COD) for obtaining the SIFs of the interfacial cracks will be proposed.

Just mention a few of those procedures using FE analysis, Matos et. al. [7] proposed a numerical method using FE analysis to compute the SIFs of an interface crack. This method is based on the evaluation of the J-integral by the virtual crack extension method. Then, individual stress intensities were obtained from further calculations of J perturbed by small increments. Chow and Atluri [8] got the SIFs of the interfacial cracks using the virtual crack closure integral with relatively coarse finite element meshes. In their procedure, the strain energy release rates should be computed in advance using the method proposed by Rybicki and Kanninen [9] as well as Raju [10]. Sun and Qian [11] used finite elements in conjunction with the crack closure method to obtain strain energy release rates [12] from which the SIFs could then be derived. The aforementioned procedures resorted to the use of the strain energy release rate to produce the final SIFs. Yuuki and Cho [13] determined the SIFs of the interface cracks by means of the extrapolation of the crack surface displacement. In this method, it needs skills to select the effective data area to determine the slope of the extrapolated line. Oda et al. [14] obtained the SIFs of the interface cracks using the ratios of the crack tip stresses. His concept was extended from the crack tip stress method proposed by Teranishi and Nisitani [15] for the homogeneous cracks. Noda and Lan [16] investigated the robustness of Oda's method and proposed a linear extrapolation technique to improve the accuracy. However, both the very refined meshes and the extrapolation technique add to the extra computational costs which lead to the lower efficiency.

As aforementioned, Oda's method [14] does not directly give accurate results for the deep crack case as well as the strong material mismatch situations. Furthermore, FE element type and the grid size also affect the accuracy to some extent. Therefore, in this research, the authors tend to use the ratio of the relative crack opening displacement (COD) behind the crack tip to improve the accuracy. The robustness of the current procedure is investigated by a convergence study on the element type adaptability and mesh size dependency. It is found that the oscillatory singularity is successfully avoided by investigating the CODs of the FE nodes behind the crack tip instead of using the crack tip stresses. Meanwhile, the procedure for treating the case where the reference and the given unknown problems have different crack lengths is also depicted to deduce the modeling time. Therefore, the current procedure can give reliable results with rather coarse meshes more effectively and rapidly.

Fig.1

2. Analysis Method

2.1 Formulation for the interface crack problems

Consider two isotropic elastic materials joined along the x-axis as indicated in Fig.1 with material 1 above the interface and material 2 below. The stress distributions along the interface are defined as shown in Eq.(1) [17] .

$$\sigma_y + i\tau_{xy} = \frac{K_I + iK_{II}}{\sqrt{2\pi r}}\left(\frac{r}{2a}\right)^{i\varepsilon}, \quad r \to 0 \tag{1}$$

here, σ_y, τ_{xy} denote the normal and shear stress components near the crack tip respectively, r is the radial distance behind the crack tip, a is the half crack length and ε is the bi-elastic constant given by:

$$\varepsilon = \frac{1}{2\pi}\ln\left[\left(\frac{\kappa_1}{\mu_1} + \frac{1}{\mu_2}\right)\Big/\left(\frac{\kappa_2}{\mu_2} + \frac{1}{\mu_1}\right)\right] \tag{2}$$

$$\kappa_m = \begin{cases} 3 - 4\nu_m & (plane\ strain) \\ 3 - \nu_m / 1 + \nu_m & (plane\ stress) \end{cases} \tag{3}$$

where $\mu_m\ (m = 1, 2)$ and $\nu_m\ (m = 1, 2)$ are the shear moduli and Poisson's ratios of either respective materials. The associated crack flank displacements $\delta_{\mathrm{d}} = u_d(r, \theta = \pi) - u_d(r, \theta = -\pi), (d = x, y)$ for nodes i, i' at a distance r behind the crack tip shown in Fig. (1), are given by [18]

$$\delta_y + i\delta_x = \frac{K_I + iK_{II}}{2(1 + 2i\varepsilon)\cosh(\varepsilon\pi)}\left[\frac{\kappa_1 + 1}{\mu_1} + \frac{\kappa_2 + 1}{\mu_2}\right]\left(\frac{r}{2\pi}\right)^{1/2}\left(\frac{r}{l}\right)^{i\varepsilon} \tag{4}$$

where l is an arbitrary reference length which scales with specimen size or crack length, for the definition of Eq.(1), we have $l = 2a$ without loss of generality.

Considering $(r/l)^{i\varepsilon} = \cos(\varepsilon\ln(r/l)) + i\sin(\varepsilon\ln(r/l))$ and rearranging Eq.(4), then the stress intensity factor components K_I, K_{II} can be separated as :

$$K_I = S\left\{(\delta_y - 2\varepsilon\delta_x)\cos\left[\varepsilon\ln\left(\frac{r}{l}\right)\right] + (\delta_x + 2\varepsilon\delta_y)\sin\left[\varepsilon\ln\left(\frac{r}{l}\right)\right]\right\} \tag{5}$$

$$K_{II} = S\left\{(\delta_x + 2\varepsilon\delta_y)\cos\left[\varepsilon\ln\left(\frac{r}{l}\right)\right] - (\delta_y - 2\varepsilon\delta_x)\sin\left[\varepsilon\ln\left(\frac{r}{l}\right)\right]\right\} \tag{6}$$

and

$$S=\frac{2\cosh(\varepsilon\pi)\left(r/2\pi\right)^{-1/2}}{\left(\frac{\kappa_1+1}{\mu_1}+\frac{\kappa_2+1}{\mu_2}\right)} \tag{7}$$

we can rewrite Eq.(5)and(6) as

$$\frac{K_I}{\delta_y}=S\left\{\left(\cos Q+2\varepsilon\sin Q\right)+\left(\sin Q-2\varepsilon\cos Q\right)\frac{\delta_x}{\delta_y}\right\} \tag{8}$$

$$\frac{K_{II}}{\delta_x}=S\left\{\left(\cos Q+2\varepsilon\sin Q\right)-\left(\sin Q-2\varepsilon\cos Q\right)\frac{\delta_y}{\delta_x}\right\} \tag{9}$$

and

$$Q=\varepsilon\ln\left(r/l\right) \tag{10}$$

From Eq.(8) and (9), when $Q,\varepsilon,\delta_y/\delta_x$ are kept the same for two different interface cracks, then we get a relationship as

$$K_I/\delta_y=const,\ K_{II}/\delta_x=const \tag{11}$$

Considering two interface crack problems A and B (say, problems in Fig.2), by satisfying the preconditions as shown in Eq.(12) and (13), then the stress intensity factors K_I, K_{II} behave proportional relationship with δ_y,δ_x as depicted in Eq.(14). Where, the relative crack opening displacement δ_y,δ_x can be computed by FE analysis, assuming one of the two problems is analytically well solved in advance, say, K_I, K_{II} of problem A are given in advance, then the SIFs of problem B can be easily obtained from Eq.(14).

$$\begin{pmatrix} Q_A=Q_B \\ \varepsilon_A=\varepsilon_B \end{pmatrix}\rightarrow\begin{pmatrix} \left[\varepsilon\ln\left(r/l\right)\right]_A=\left[\varepsilon\ln\left(r/l\right)\right]_B \\ \varepsilon_A=\varepsilon_B \end{pmatrix} \tag{12}$$

$$\left[\delta_y/\delta_x\right]_A=\left[\delta_y/\delta_x\right]_B \tag{13}$$

$$\left[K_I/\delta_y\right]_{\mathrm{A}}=\left[K_I/\delta_y\right]_{\mathrm{B}},\left[K_{II}/\delta_x\right]_A=\left[K_{II}/\delta_x\right]_B \tag{14}$$

and the strain energy release rate for the crack advance in the interface is

$$G=\frac{1}{16\cosh^2(\varepsilon\pi)}\left[\frac{\kappa_1+1}{\mu_1}+\frac{\kappa_2+1}{\mu_2}\right]\left(K_I^2+K_{II}^2\right) \tag{15}$$

Fig.2

2.2 Application of the proportional COD method

The problem that SIFs have been solved in advance can be treated as the reference. Therefore, a central cracked dissimilar bonded half-planes subjected to remotely uniform tensile and shear stresses as shown in Fig.2(a) is selected as the reference problem for generality. Its analytical solution was firstly derived by Rice and Sih [19], and takes the form

$$K_I^*+iK_{II}^*=\left(\sigma_y^\infty+i\tau_{xy}^\infty\right)\sqrt{\pi a}\left(1+2i\varepsilon\right) \tag{16}$$

where an asterisk (*) is employed to denote the SIFs for the reference problem. σ_y^∞, τ_{xy}^∞ are the remote uniform tension and shear applied to the bonded half-planes. a is the half crack length of the center crack. Furthermore, the transversal tension $\sigma_{x1}^\infty,\sigma_{x2}^\infty$ in Fig.2(a) behave

$$\sigma_{x2}^\infty=\frac{1}{1+\kappa_2}\left[\frac{\mu_2}{\mu_1}\left(1+\kappa_1\right)\sigma_{x1}^\infty+\left\{3-\kappa_2-\frac{\mu_2}{\mu_1}\left(3-\kappa_1\right)\sigma_y^\infty\right\}\right] \tag{17}$$

As aforementioned, the preconditions in Eq.(12) and (13) should be firstly met to ensure the current method available. Eq.(12) can be easily satisfied by making the bi-elastic constant ε and the relative distance behind the crack tip r/l the same for the two problems. Here, some extra techniques should be employed to make Eq. (13) satisfied. We consider the reference problem shown in Fig.2(a), the relative COD δ_y,δ_x can be solved in an indirect manner using the principle of linear superposition. As schematically shown in Fig.3, the reference problem (Problem A) can be solved in two steps (ProblemA1 and A2). Namely, they are Problem A1 in Fig.3 subjects to pure remote tension T and Problem A2in Fig. Three subjects to pure remote shear S. Let $\delta_{y,A}^*,\delta_{x,A}^*$ denote the COD of Problem A subjected to combined T,S, $\delta_{y,A1}^{T=1*},\delta_{x,A1}^{T=1*}$ denote those of Problem A1 subjected to pure unit tension $T=1$, and $\delta_{y,A2}^{S=1*},\delta_{x,A2}^{S=1*}$ denote those of Problem A2 subjected to pure unit shear $S=1$, respectively. Using the theory of linear superposition, then the relative CODs $\delta_{y,A}^{*},\delta_{x,A}^{*}$ of the reference problem (Problem A) take the following form

$$\delta_{y,A}^{*}=\delta_{y,A1}^{T=1*}\times T+\delta_{y,A2}^{S=1*}\times S \tag{18}$$

$$\delta_{x,A}^{*}=\delta_{x,A1}^{T=1*}\times T+\delta_{x,A2}^{S=1*}\times S \tag{19}$$

Recall Eq.(13) and substitute δ_y,δ_x with $\delta_{y,A}^{*},\delta_{x,A}^{*}$ for problem A, then we have

$$\left[\frac{\delta_{y,A}^{*}}{\delta_{x,A}^{*}}\right]_A=\left[\frac{\delta_{y,A1}^{T=1*}\times T+\delta_{y,A2}^{S=1*}\times S}{\delta_{x,A1}^{T=1*}\times T+\delta_{x,A2}^{S=1*}\times S}\right]_A=\left[\frac{\delta_{y,B}}{\delta_{x,B}}\right]_B \tag{20}$$

Rearranging Eq.(20) gives the solution of S/T,

$$S/T=\frac{\delta_{x,B}\cdot\delta_{y,A1}^{T=1*}-\delta_{y,B}\cdot\delta_{x,A1}^{T=1*}}{\delta_{y,B}\cdot\delta_{x,A2}^{S=1*}-\delta_{x,B}\cdot\delta_{y,A2}^{S=1*}} \tag{21}$$

Using T,S in Eq.(21) as the boundary condition for Problem A, then Eq.(13) is satisfied and eventually Eq.(14) sets up. Finally, the SIFs for the target unknown problem (problem B) can be yielded using the proportional relationship as given in Eq.(22).

$$K_{I,B}=\frac{\delta_{y,B}}{\delta_{y,A}}\times K_{I,A},\ K_{II,B}=\frac{\delta_{x,B}}{\delta_{x,A}}\times K_{II,A} \tag{22}$$

Fig.3

2.3 Formulation for the problems with different crack lengths

Recall Eq.(1) and (4), the aforementioned proportional COD method only sets up when the reference lengths ($l=2a$) are set the same for the problems A and B. New FE models for the reference should be repeatedly created each time when the crack length of the given unknown problem changes. This means quite a lot computational costs in the practical application. Consider the case where the reference problem A and the given unknown problem B have different crack lengths a_A and a_B.Then the SIFs of Problem B should be computed according to the following process.

1.The FE mesh patterns and the minimum element size around the crack tip are kept the same for the two problems A and B. Then, node pairs $i, i^{'}$ of problem A and B in Fig. 4 will be used for the computation.

2. Calculating the SIFs $K_I^{'}, K_{II}^{"}$ using the aforementioned proportional COD method by assuming the same reference length $l = 2a_1$ for the given unknown problem B. Here, $K_I^{'}, K_{II}^{"}$ denote the SIFs of Problem B with a reference length $l = 2a_1$.

3. Revising the computed SIFs by a constant phase factor which is introduced by the difference of the reference crack lengths. Let K_I, K_{II} denote the SIFs of the given unknown problem with different reference lengths $l = 2a_2$, then K_I, K_{II} with the reference lengths $l = 2a_2$ can be expressed as

$$\begin{pmatrix} K_I \\ K_{II} \end{pmatrix} = \begin{vmatrix} \cos\left[\varepsilon \ln\left(\dfrac{a_2}{a_1}\right)\right] & -\sin\left[\varepsilon \ln\left(\dfrac{a_2}{a_1}\right)\right] \\ \sin\left[\varepsilon \ln\left(\dfrac{a_2}{a_1}\right)\right] & \cos\left[\varepsilon \ln\left(\dfrac{a_2}{a_1}\right)\right] \end{vmatrix} \begin{pmatrix} K_I^{'} \\ K_{II}^{"} \end{pmatrix} \tag{23}$$

In the practical application, the current method is fairly efficient since only one FE model of the reference problem is necessary for all the unknown problems with different crack lengths.

Fig. 4

3 Method robustness and convergence study

In this section, the efficiency and accuracy of the current procedure will be demonstrated by pursuing a convergence study. The mesh-size dependency, the location of the nodes selected for computation and the mesh adaptability will also be investigated and depicted.

Fig.5

3.1 Specifications and configurations of the FE models

The MSC.MARC 2007 [20] finite element analysis package is used to compute the COD in this research. Fig.5(a) shows the FE model geometric configurations for the reference problem A. The crack length is set to $2a = 2mm$. It should be noted that the relative COD values for the reference problem converge as the width of the model is larger than 1500 times the crack length a. Then a plate width of $W = 1620 \times 2a = 3240mm$ and a length of $L = 2W = 6480mm$ are used to model the reference problem A ($L = 2W, W/a = 1620$). Fig.5(b) shows the FE model geometric configuration for a single-edge cracked bonded strip (an example for the given unknown problem B). The crack length for the given unknown problem B is fixed to $a = 1mm$ which is the half crack length of the reference problem A. The width of the bonded strip W varies from $a/W = 0.1 \sim 0.9$, the length L is assumed to be much greater than the width W ($L = 2W$ is assumed in the FE model). Furthermore, the minimum finite element sizes $e_{\min}$ are kept the same for the reference and the given unknown problems.

Fig.5(c) shows the FE mesh pattern around the singular region. The singular region around the crack tip are well refined in a self-similar manner by increasing the number of layers, and the element size for each inferior layer is one-third of the superior one. The meshes are made of 4-node/8-node quadrilateral elements in plane stress or plane strain conditions. Furthermore, the meshes of the reference problem A and the given unknown problem B are kept the same to make sure a high computational accuracy. It should be noted that although highly accurate δ_y, δ_x near the crack tip cannot be obtained by FE analysis. The ratios δ_y / δ_x are fairly accurate since the same FE meshes and model density are assumed in the computation.

3.2 Determination of the location of the nodes used for computation

Fig.6

The computational accuracy is investigated for an edge-cracked bonded strip shown in Fig.2(b) by varying the node position behind the crack tip. Fig. 6 shows a finite element idealization with linear quadrilateral elements. The SIFs are computed using different pairs of nodes (say, i, i' and j, j' et al.) and for four cases of minimum element size ($e_{\min} = 2a/3^3, 2a/3^4, 2a/3^5, 2a/3^6$). The material combinations are fixed to $E_1/E_2 = 100, \nu_1 = \nu_2 = 0.3$, and the relative crack length $a/W = 0.1$. The SIFs are normalized by $\sigma\sqrt{\pi a}$ as depicted in Eq. (24) and are plotted against the node position behind the crack tip in Fig. 7(a) and (b), respectively.

$$F_I = K_I / \sigma\sqrt{\pi a}, F_{II} = K_{II} / \sigma\sqrt{\pi a} \tag{24}$$

It can be seen that for all types of minimum element size, the SIFs behave linearity with the distance from the node pairs selected in the computation to the crack tip. The normalized SIFs F_I and F_{II} approach the published data 1.251 and 0.424 obtained by Miyazaki et al. [21] and Matsumto et al.[22]. The closer the distance between the node pairs used in the computation and the crack tip, the more accurate the results are. The refined meshes also contribute to a better computational accuracy. However, it should be noted that the nodes within the oscillatory singularity zone are not recommended in the computation. Furthermore, the current method is less sensitive to the FE mesh size. Therefore, unless otherwise specified in this paper, all the node pairs used in the computation are those who are closest to the crack tip but not located within the oscillatory singularity zone to improve the accuracy.

Fig. 7

3.3 Convergence studies for mesh-size dependency

Fig. 8

It suggests that the discretization in the near-tip region has an important role in the accuracy of the FE method. The accuracy must be balanced with the computational efficiency by investigating the total number of elements required. Here, a convergence study is carried out to investigate the effects of the minimum element size $e_{\min}$ and the model density on the accuracy. Different FE models using the 4-node quadrilateral elements and the 8-node parabolic quadrilateral elements as well as using 6 different minimum element sizes are tested. The mesh pattern, model density and minimum element size for each pair of models are fixed the same. Namely, the minimum element size for each pair of models is $a/3^3, a/3^4, a/3^5, a/3^6, a/3^7, a/3^8$ which corresponding to the total number of mesh layers $NL = 7,8,9,10,11,12$, respectively. Without loss of generality, a material combination $G_1/G_2 = 100, \nu_1 = \nu_2 = 0.3$ and plane stress condition are assumed for an edge interface crack $a/W = 0.2$. Similar conclusions can also be found from other cases. The results F_I and F_{II} are plotted in Fig. 8(a) and (b), respectively. It can be seen that the normalized SIFs converge with deceasing the minimum element size. F_I converge when $e_{\min} < a/3^4$, and F_{II} converge when $e_{\min} < a/3^5$. The relative higher error for F_{II} is believed to be purely numerical resulting from a small F_{II} value. It can be concluded that the current method does not show particularly great sensitivity with the element size. Say, F_I, F_{II} has 3-digit accuracy when $e_{min} < a/3^4$, and 4-digit accuracy when $e_{min} < a/3^5$. Furthermore, the convergence speed of the current procedure reaches the same level accuracy is faster than that of the crack tip stress method [14]. In this research, without special notification, a minimum element size of $e_{min} = a/3^5$ is selected to obtain a better tradeoff between computational cost and accuracy.

3.4Mesh adaptability and element type dependency

It is known that the higher order elements can better catch the stress singularity in the FE analysis. In order to investigate the effect of the element type dependency, the two-dimensional single-edge cracked bonded strip shown in Fig.2(b) is computed using 3 different types of finite elements. The material combinations $E_1/E_2 = 4, \nu_1 = \nu_2 = 0.3$ and plane stress condition are assumed in the computation, the minimum element size is fixed to $e_{min} = a/3^6$. Four different cases of nodes and element types as tabulated in Table 1 are investigated and compared in the analysis. Namely, they are Nodes i and i' of the3-node triangle element in Fig. 9(a), nodes i and i' of the 4-node linear quadrilateral element in Fig. 9(b), the corner nodes j and j' of the 8-node parabolic quadrilateral element in Fig. 9(c) and mid-side nodes i and i' of the 8-node parabolic element in Fig. 9(c). Furthermore, it is known that SIFs vary greatly and decrease with the reducing of the relative crack length a/W under the same loading conditions. Oda [14] pointed out that the relative crack length has an effect on the accuracy of the extended crack tip stress method, and the absolute error is believed to be considerable large for the deep crack case. Therefore, we used the same a/W to be able to compare our results with those predicted by other researchers to investigate the crack size effect. In this research, all the relative crack lengths a/W of different crack problems vary from 0.1 to 0.9 with an increasing step of 0.1, then we can investigate the robustness and accuracy from the shallow crack case to the very deep crack case.

The intermediate relative COD results for each case are presented in Table 2, and their final F_I, F_{II} results are listed in Table 3. It can be seen from these tables that F_I, F_{II} are in good agreement for different types of FE element, though their FE intermediate values δ_I, δ_{II} exhibit significant differences, and F_I, F_{II} of the current method agree well with those published data by Miyazaki [21] for $a/W = 0.1 \sim 0.8$. Furthermore, the current procedure gives reliable results independent of the relative crack length. This leads us to a conclusion that though the intermediate relative CODs obtained from FEA may be different for various element types, the final results agree quite well. The current method resorts to the selection of the CODs instead of the crack-tip stresses to avoid the strong singularity, and consequently aids to reduce the numerical error and produce the optimal K_I, K_{II} results. Therefore the proposed proportional COD method can determine K_I, K_{II} with extremely high accuracy. It should also be noticed that the current procedure can give reliable computational accuracy without using too much refined meshes. Moreover, it also exhibits good FE mesh type adaptability and higher computing efficiency.

Fig. 9
Table 1
Table 2
Table 3

4 Numerical results

4.1Homogeneous crack subjected to tensile and bending loadings

In the aforementioned discussion, when $\varepsilon = 0$, it is analogous to that of a crack in a homogeneous material. In this case, the oscillatory singularity vanishes and the stress field becomes square-root singular. Therefore, the current procedure should also be applicable to the homogeneous crack. The first example considered here is an edge cracked panel subjected to tensile and bending loads as shown in Fig. 10(a). Fig. 10(b) and (c) show the tension applied at the top and bottom boundaries to counter the tensile load and the bending moment applied to the homogeneous plate, respectively. The crack length is set to $\mathrm{a} = 1mm$ and the size of the panel varies for a range of $\mathrm{a}/W = 0.1 \sim 0.9$. The mesh pattern, model density and minimum element size are fixed the same as discussed above, 8-node quadrilateral element is employed in the computation. The normalized SIFs computed by the present method are tabulated and compared to those predicted by Kaya and Erdogan[23] and Noda et al.[24] in Table 4. It can be seen that the results and those of Kaya and Erdogan[23] as well as Noda et al. [24] are in very good agreement for the two loading conditions. Specifically, the errors are within 0.1% for both the two loading conditions.

Fig. 10
Table 4

4.2Interfacial cracks subjected to tension

The second example is the two-dimensional plane-stress problems of a central interface crack and an edge interface crack. The FE models are built in a similar manner as depicted in Section 3.1. The crack length is set to $a = 1mm$ and the width of the bonded strip varies from $a/W = 0.1 \sim 0.9$. The length is set to 2 times the width of the bonded strip. The same elastic parameters $E_1/E_2 = 2, 4, 10, 100, \nu_1 = \nu_2 = 0.3$ and the plane stress condition which were adopted by other researchers [13,21,22] are assumed in the computation. Their Dundurs' parameters α, β are plotted in the half $\alpha - \beta$ space in Fig. 11 together with those of some typical engineering materials complied by Suga et al. [25]. As can be seen from Fig. 11, the elastic parameters used in the computation are representative since their α, β are widely distributed along the densely distributed area for the typical engineering materials. The computed SIFs are also normalized by $\sigma\sqrt{\pi a}$, and they are tabulated in Table 5 together with those predicted by Matsumto et al.[22], for the central and edge interface crack problems respectively. As shown in this table, the results of the current procedure coincide with those predicted by Matsumto et al.[22]. Specifically, the largest errors of the strong material mismatch and the relative deep crack cases are within 0.2% for the center interface crack case, and those of the edge interface crack are less than 0.5%. It can be found that the deep crack length and the strong material mismatch do not affect the computational accuracy. Therefore, the current procedure is generic, and it can get accurate SIFs more effectively without using high model density or any post-processing techniques. Furthermore, it is known that the SIFs do not behave simple uniform varying relationship with α, β and a/W [26]. However, the SIFs in Table 5 increase monotonically with the increment of E_1/E_2, since ν_1, ν_2 are kept the same and the plane stress condition is assumed in the analysis. This leads us to a conclusion that the SIFs grows with the stronger material mismatch for this specific condition.

Table 5

Table 6

4.3Axisymmetrical crack problems in a cylindrical bar

To thoroughly assess the mesh dependence and the applicable possibility on treating the case where the reference problem and the given unknown problem have different FE models, anaxisymmetrical3-D crack, a penny-shaped crack and a circumferential surface crack are analyzed in this section. The calculated SIFs are compared with those from the literature. Requirements of the mesh patterns are further investigated and discussed. Similarly, the 8-node quadrilateral element in plane strain condition is used in building the reference problem, and two different mesh types as the 8-node axisymmetric solid element and 8-node hexahedral solid element are used to mesh the penny-shaped and circumferential surface crack problems as shown in Fig.12(a) and (b), respectively. The 2-D axisymmetric model is refined in a similar way as shown in Fig.5(c), and the 3-D FE model idealizations and its boundary conditions are demonstrated in Fig.12(c). The normalized SIFs for the penny-shaped and circumferential cracks as well as those predicted by Benthemand Koiter [27] and Nisitani and Noda[28] are tabulated and compared in Table 6, respectively. It can be seen from this table that the normalized SIFs computed by the axisymmetric models coincide with those predicted by 3-D solid models. Furthermore, the SIF values of the penny-shaped crack predicted by the current method are in good agreement with those by Benthem and Koiter [27], and the largest error is around 0.7% for the deep crack case. For the circumferential surface crack, the values of the current procedure coincide with those predicted by Nisitani and Noda [28] with the largest error within 0.1%. This means the current method is also useful for the axisymmetrical crack problems, and the computational accuracy of the current method is independent of the FE element types for the reference and target unknown problems.

Fig.11
Table 7

5. Conclusions

In this paper, the proportional relative crack opening displacement (COD) behind the crack tip was employed based on the crack tip stress method to compute the stress intensity factors. The robustness of the current procedure was investigated by a convergence study. It was found that the current procedure gave reliable results with rather coarse meshes more effectively and rapidly, and it exhibited good element type adaptability and less mesh dependency. Furthermore, the accuracy was also tested via several numerical examples. It was confirmed that resorting to the selection of the COD values behind the crack tip instead of the direct crack tip stresses could avoid the strong singularity, and aid to produce a better accuracy. Comparing with that of the crack tip stress method, the accuracy was not affected by the relative deep crack and the strong material mismatch. Meanwhile, a procedure on treating the case where the reference problem and the given unknown problem have different crack lengths was also depicted to reduce the modeling time. Therefore, the current method is fairly efficient and can be used as an effective tool in the reliability analysis of the bonded multi-layers.

Acknowledgements

The authors would like to thank Professor Kazuhiro Oda for the discussions which have greatly influenced this research. This work was supported in part by grants from National Natural Science Foundation of China (NSFC) (No. 51376111) and the Fundamental Research Funds of Shandong University (No. 31380076614017).

References

[1] Williams ML. The stresses around a fault or crack in dissimilar media. Bull Seismol Soc Am 1959; 49c:199–204.

[2] Rice JR, Sih GC. Plane problems of cracks in dissimilar media. J Appl Mech 1965;32:418-423.

[3] Erdogan F. Stress distribution in a nonhomogeneous elastic plane with cracks. J Appl Mech 1963;30:232–236.

[4] Erdogan F. Stress distribution in bonded dissimilar materials with crack. J Appl Mech 1965;32:403–409.

[5] England AH. A crack between dissimilar media. J Appl Mech 1965;32:400–402.

[6] Willis JR. Crack Propagation in Viscoelastic Media. J Mech Phys Solids l967;15:229-240.

[7] Matos PPL, McMeeking RM, Charalambides PG and Drory MD. A method for calculating stress intensities in bimaterial fracture. Int J Frac 1989;40:235-254.

[8] Chow WT, Atluri SN. Finite element calculation of stress intensity factors for interfacial crack using virtual crack closure integral. Comput Mech 1995;16:417-425.

[9] Rybicki EF, Kanninen MF. A finite element calculation of stress intensity factors by a modified crack closure integral. Eng Fract Mech 1977;9:931-938.

[10] Raju IS. Calculation of strain-energy release rates with higher order and singular finite elements. Eng Fract Mech 1987;28:251-274.

[11] Sun CT, Qian W. The use of finite extension strain energy release rates in fracture of interfacial cracks. Int J Solids Struct 1997;34:2595-2609.

[12] Jih CJ, Sun CT. Evaluation of a finite element based crack-closure method for calculating static and dynamic strain energy release rates. Eng Fract Mech 1990;37:313-322.

[13] Yuuki R, Cho SB. Efficient boundary element analysis of stress intensity factors for interface cracks in dissimilar materials. Eng Fract Mech 1989;34:179-188.

[14] Oda K, Noda NA and Atluri SN. Accurate Determination of Stress Intensity Factor for Interface Crack by Finite Element Method. Key Eng Mater 2007;353-358: 3124-3127.

[15] Teranishi T, Nisitani H. Determination of highly accurate values of stress intensity factor in a plate of arbitrary form by FEM. Trans JSME (in Japanese) 1999;65:16-21.

[16]Noda NA, Lan X. Stress intensity factors for an edge interface crack in a bonded semi-infinite plate for arbitrary material combination. Int J Solids Struct 2012;49:1241-1251.

[17] Malysev BM, Salganik RL. The strength of adhesive joints using the theory of cracks. Int J Fract 1965;1:114-127.

[18] Rice JR. Elastic fracture mechanics concepts for interfacial cracks. J Appl Mech 1988;55:98-103.

[19] Rice JR, Sih GC. Plane Problems of Cracks in Dissimilar Materials. J Appl Mech

1965;32:418-423.

[20] MSC Marc 2007. MSC Marc 2007 User's Guide. MSC.Software Corp: California, USA; 2007.

[21] Miyazaki N, Ikeda T, Soda T, Munakata T. Stress intensity factor analysis of interface crack using boundary element method-Application of contour-integral method. Eng Fract Mech 1993;45:599-610.

[22] Matsumto T, Tanaka M, Obara R. Computation of stress intensity factors of interface cracks based on interaction energy release rates and BEM sensitivity analysis. Eng Fract Mech 2000;65:683-702.

[23] Kaya AC, Erdogan F. On the solution of integral equations with strongly singular kernels. Q Appl Math 1987;45:105-122.

[24] Noda NA, Araki K, Erdogan F. Stress intensity factors in two bonded elastic layers with a single edge crack under various loading conditions. Int J Fract 1992;57: 101-126.

[25] Suga T, Elssner G, Schmauder S. Composite parameters and mechanical compatibility of material joints. J Compos Mater 1988;22:917-934.

[26] Lan X, Noda NA, Mithinaka K, Zhang Y. The effect of material combinations and relative crack size to the stress intensity factors at the crack tip of a bi-material bonded strip. Eng Fract Mech 2011;78:2572-2584.

[27] Benthem JP, Koiter WT. Method of analysis and solutions of crack problems. In: Sih GC, editors. Mechanics of fracture. Leyden: Noordhoff Int Publishing; 1973, p.131-178.

[28]Nisitani H, Noda NA. Proc Int Conf Appl Fract Mech Mat Struct. 1984:519-523.

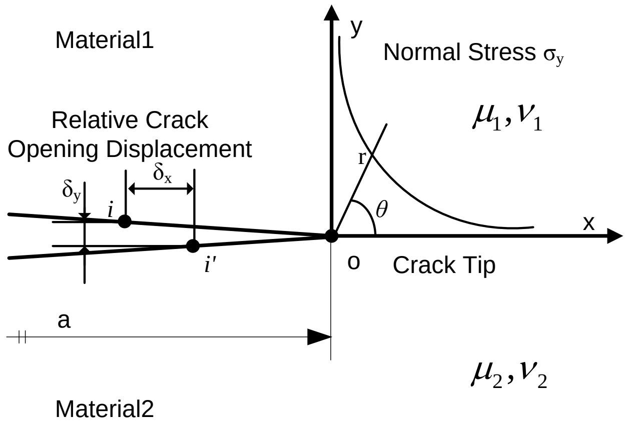

Fig.1. Stress distribution and relative crack displacement of an interface crack

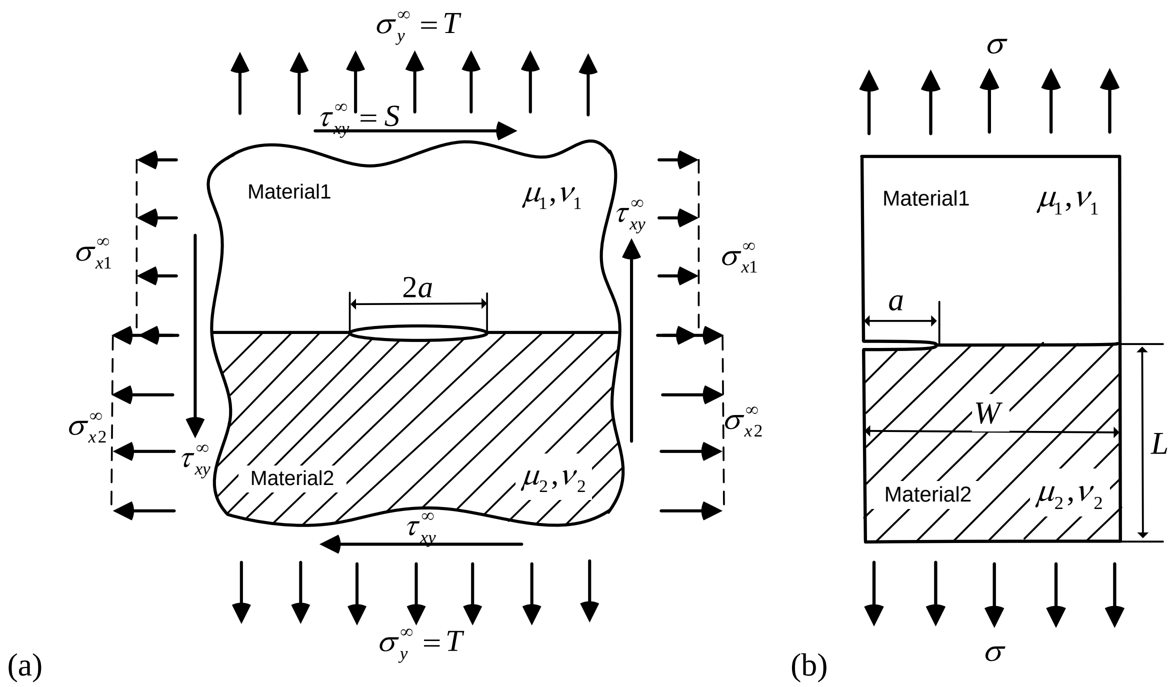

Fig.2. Geometric configuration for (a) the reference problem A and (b) the given unknown problem B

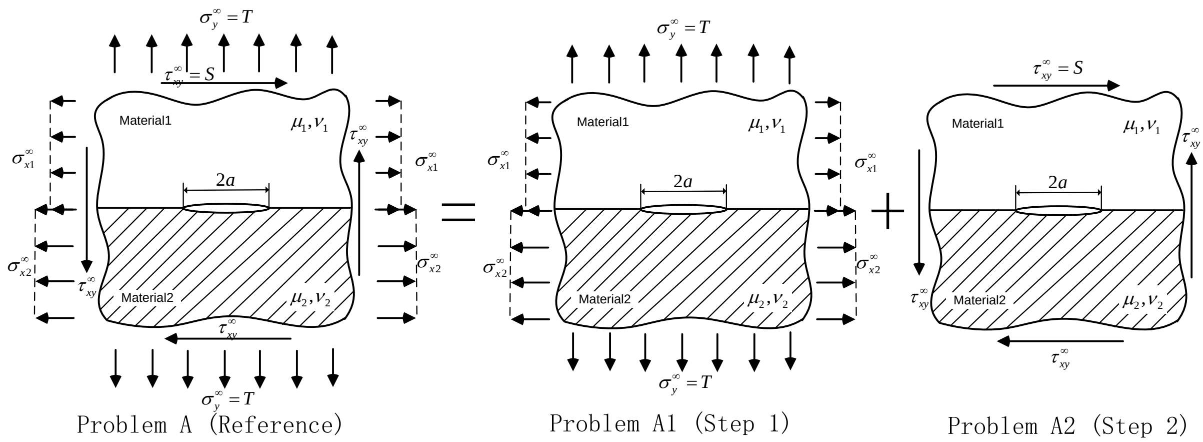

Fig.3. Schematic representation of superposition method for the reference problem

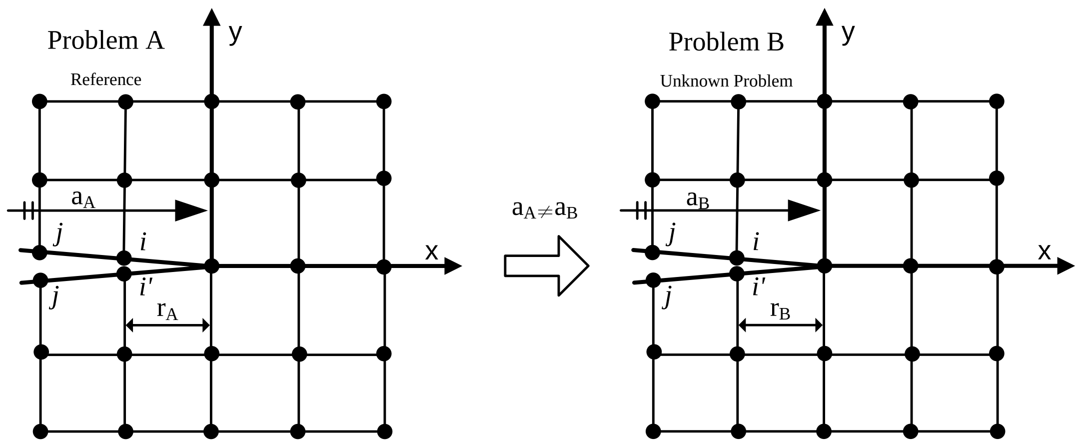

Fig. 4. FE model idealizations for node scheme of Problem A and B

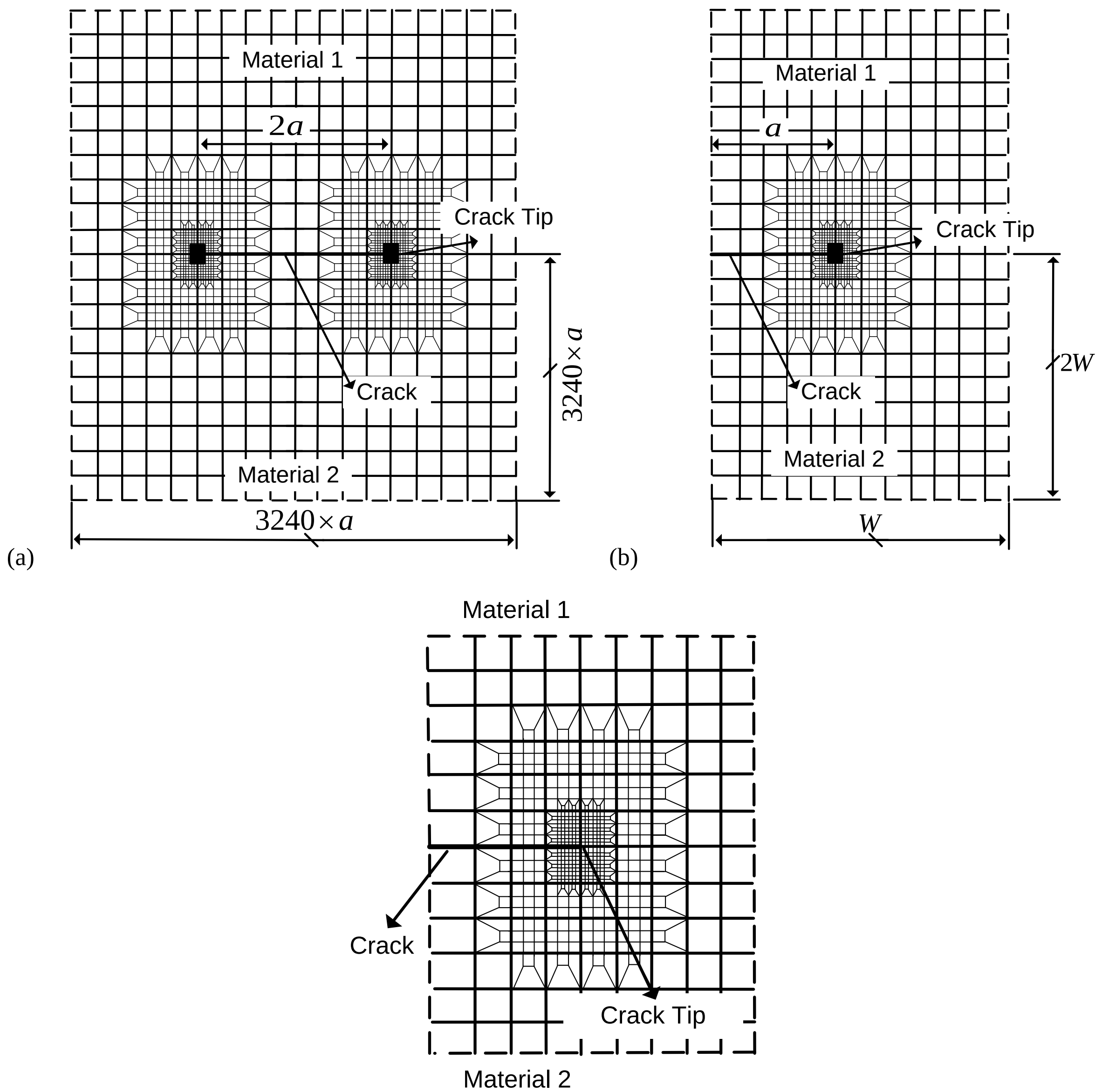

Fig.5. FE model geometric configurations for (a) the reference problem and (b) the given unknown problem and (c) the FE mesh schematic in the singular region

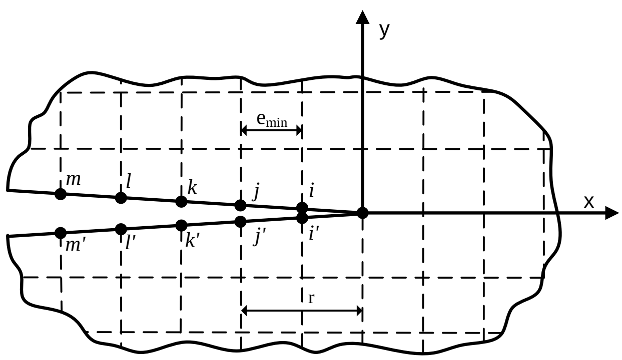

Fig.6. Finite element idealization around the crack tip

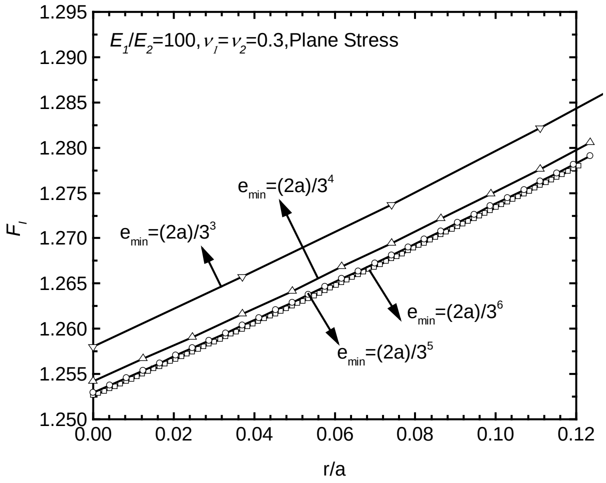

(a)

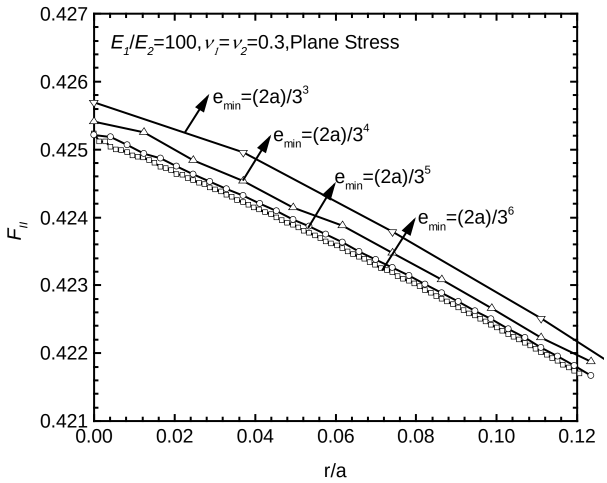

(b)

Fig. 7. Normalized SIFs (a) F_I and (b) F_{II} computed using nodes of various positions behind the crack tip

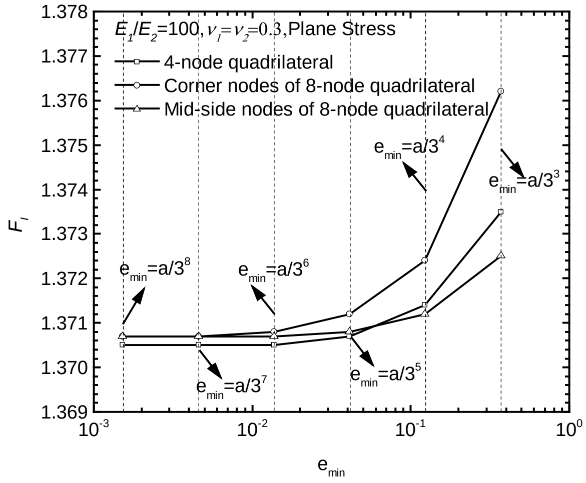

(a)

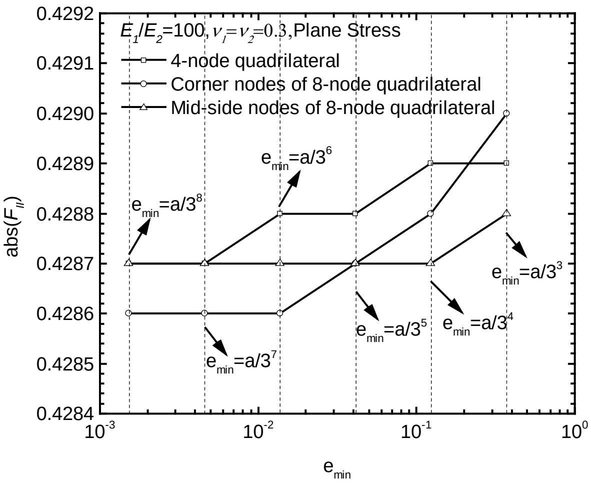

(b)

Fig. 8. (a) Convergence study for (a) F_I and (b) F_{II} with varying the minimum element size

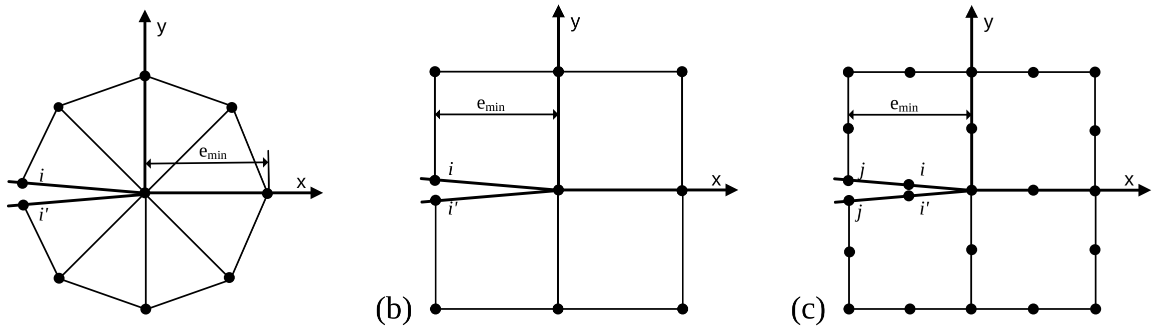

(a) (b) (c)

Fig. 9. Non-singular elements around the crack tip (a) 3-node linear triangular element (b) 4-node linear quadrilateral element and (c) 8-node parabolic quadrilateral element

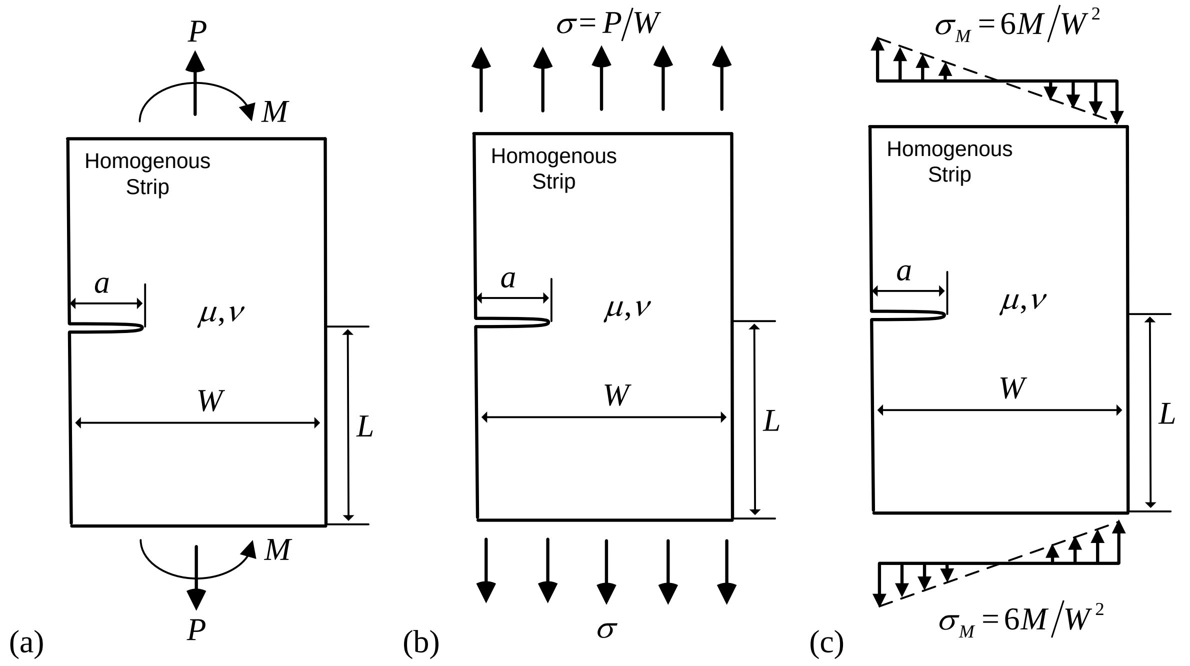

Fig. 10. (a) A single-edge-cracked homogenous strip subjected to tensile and bending loading conditions, tensions at the boundaries to counter the (b) tensile loads and (c) the bending loads

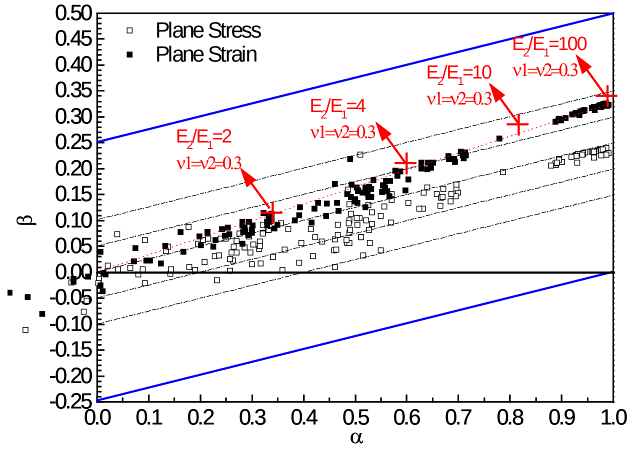

Fig. 11. Dundurs' material combinations used in the computation together with those of some typical engineering materials compiled by Suga et al.[25]

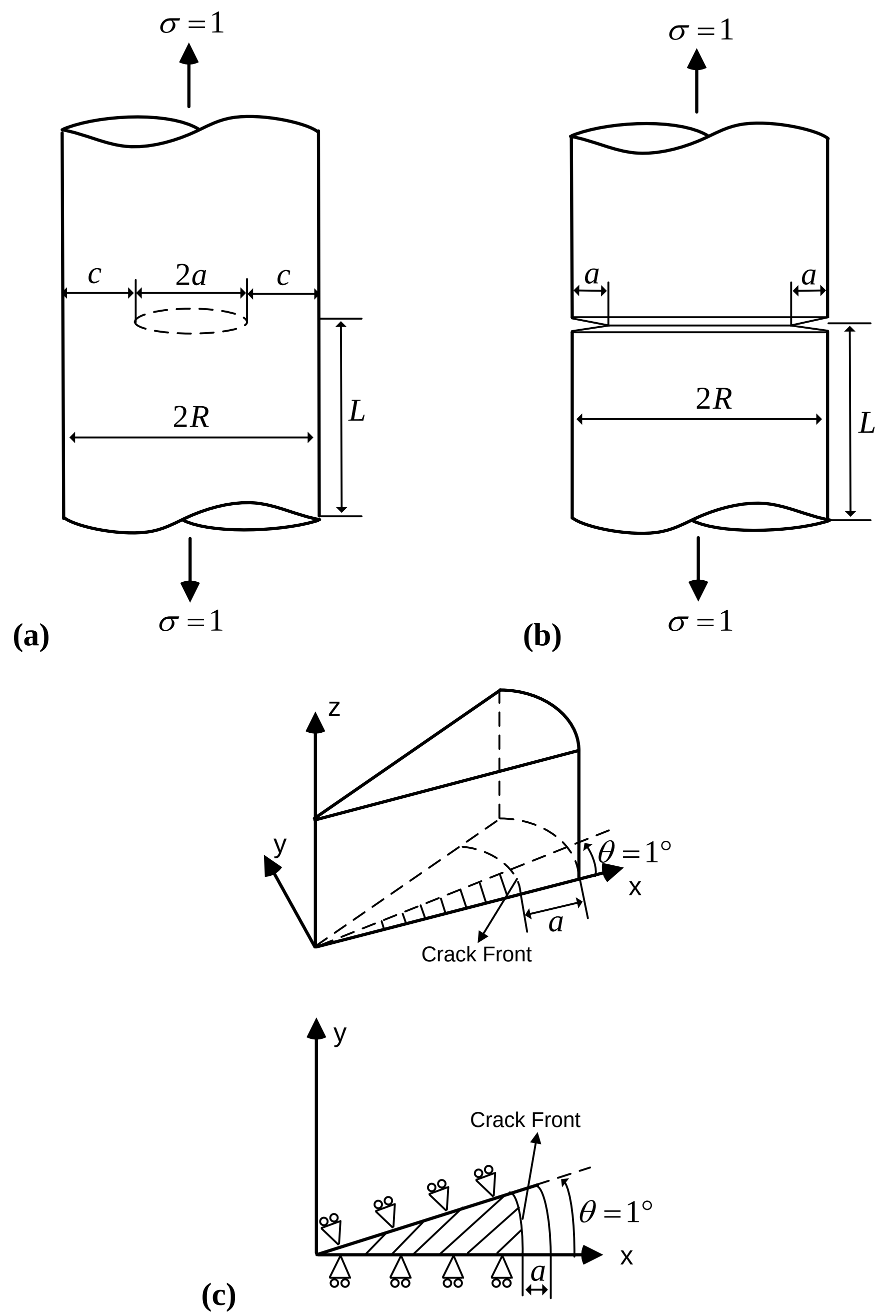

Fig.12. (a) A penny-shaped crack and (b) a circumferential surface crack in a cylindrical bar under tension (c) 3-D FE mesh geometry of the circumferential crack

Table 1 The finite element nodes and element types used in the computation

No.	Name	Nodes and element types used in the computation
1	Case 1	Nodes *i* and *i'* of the 3-node linear triangular element shown in Fig.8a
2	Case 2	Nodes *i* and *i'* of the 4-node linear quadrilateral element shown in Fig.8b
3	Case 3	Corner nodes *j* and *j'* of the 8-node parabolic quadrilateral element shown in Fig.8c
4	Case 4	Mid-side nodes *i* and *i'* of the 8-node parabolic quadrilateral element shown in Fig.8c

Table 2 The COD δ_y, δ_x for the reference and unknown problems, $E_1/E_2 = 4, \nu_1 = \nu_2 = 0.3$, Plane stress

FE Models	Relative CODδ_y				Relative CODδ_x			
	Case1	**Case2**	**Case3**	**Case4**	**Case1**	**Case2**	**Case3**	**Case4**
RefT	0.9526	1.0132	1.0430	0.6499	-0.4401	-0.4972	-0.5822	-0.3395
RefS	0.4856	0.5716	0.5958	0.4284	0.7422	0.9004	1.0606	0.5898
a/W =0.1	1.1972	1.2770	1.3153	0.8232	-0.4817	-0.5395	-0.6316	-0.3704
a/W =0.2	1.3421	1.4305	1.4738	0.9213	-0.5583	-0.6268	-0.7341	-0.4299
a/W =0.3	1.6138	1.7194	1.7715	1.1066	-0.6848	-0.7697	-0.9015	-0.5274
a/W =0.4	2.0450	2.1785	2.2446	1.4016	-0.8743	-0.9832	-1.1517	-0.6736
a/W =0.5	2.7342	2.9130	3.0024	1.8748	-1.1652	-1.3101	-1.5349	-0.8977
a/W =0.6	3.9132	4.1705	4.3007	2.6863	-1.6434	-1.8463	-2.1634	-1.2659
a/W =0.7	6.2018	6.614	6.8230	4.2648	-2.5286	-2.8358	-3.3238	-1.9467
a/W =0.8	11.7801	12.5783	12.9901	8.1284	-4.5551	-5.0913	-5.9705	-3.5033
a/W =0.9	34.7330	37.1709	38.4847	24.1098	-12.0352	-13.3628	-15.6921	-9.2413

RefT: The reference problem (Problem A1) in Fig.3 subjected to pure uniform tension.
RefS: The reference problem (Problem A2) in Fig.3 subjected to pure uniform shear.
a/W=0.1~0.9: The givenunknown problem in Fig.2(b) subjected to pure uniform tension.

Table 3 The normalized SIFs F_I, F_{II} computed usingdifferent types of finite element

a/W	F_I					F_{II}				
	Case 1	**Case 2**	**Case 3**	**Case 4**	**Miyazaki et al. [21]**	**Case 1**	**Case 2**	**Case 3**	**Case 4**	**Miyazakiet al. [21]**
0.1	1.209	1.209	1.209	1.208	1.209	-0.239	-0.239	-0.239	-0.239	-0.239
0.2	1.368	1.367	1.368	1.367	1.368	-0.251	-0.250	-0.250	-0.250	-0.250
0.3	1.653	1.653	1.654	1.653	1.654	-0.288	-0.288	-0.288	-0.288	-0.288
0.4	2.100	2.099	2.101	2.099	2.101	-0.359	-0.359	-0.359	-0.358	-0.359
0.5	2.805	2.804	2.807	2.805	2.807	-0.483	-0.483	-0.484	-0.483	-0.483
0.6	3.998	3.998	4.003	3.999	4.006	-0.716	-0.715	-0.717	-0.715	-0.716
0.7	6.286	6.285	6.296	6.287	6.304	-1.207	-1.206	-1.209	-1.205	-1.208
0.8	11.774	11.775	11.805	11.781	11.820	-2.532	-2.530	-2.538	-2.529	-2.538

Table 4 Normalized SIFs $F_I = K_I / \sigma\sqrt{\pi a}$ for Fig.10. (a)

a/W	**Uniform tension**			**In-plane bending**		
	Present	**Kaya and Erdogan [23]**	**Noda et al. [24]**	**Present**	**Kaya and Erdogan [23]**	**Noda et al. [24]**
0.1	1.189	1.1892	1.189	1.045	1.0472	1.046
0.2	1.367	1.3673	1.367	1.054	1.0553	1.054
0.3	1.659	1.6599	1.659	1.124	1.1241	1.123
0.4	2.111	2.1114	2.111	1.260	1.2606	1.259
0.5	2.824	2.8246	2.823	1.497	1.4972	1.495
0.6	4.031	4.0332	4.032	1.913	1.9140	1.913
0.7	6.352	6.3549	6.355	2.724	2.7252	2.725
0.8	11.95	11.955	11.95	4.673	4.6764	4.675
0.9	34.60	34.633	34.62	12.45	12.462	12.46

Table 5 Normalized SIFs $F_I = K_I / \sigma\sqrt{\pi a}, F_{II} = K_{II} / \sigma\sqrt{\pi a}$ for the central and edge interface crack problems

($\nu_1 = \nu_2 = 0.3$, plane stress)

E_1/E_2	a/W	**Central interface crack**				**Edge interface crack**			
		F_I		F_{II}		F_I		F_{II}	
		Present	**Matsumto et al. [22]**	**Present**	**Matsumto et al. [22]**	**Present**	**Matsumto et al. [22]**	**Present**	**Matsumto et al. [22]**
2	0.1	1.001	1.019	-0.072	-0.072	1.195	1.190	-0.129	-0.127
	0.2	1.019	1.053	-0.071	-0.070	1.367	1.367	-0.137	-0.137
	0.3	1.052	1.104	-0.071	--0.072	1.658	1.657	-0.158	-0.156
	0.4	1.103	1.180	-0.073	-0.073	2.108	2.109	-0.198	-0.195
	0.5	1.179	1.296	-0.078	-0.077	2.818	2.819	-0.267	-0.268
	0.6	1.294	1.477	-0.086	-0.084	4.021	4.024	-0.396	-0.398
	0.7	1.475	1.799	-0.101	-0.101	6.331	6.348	-0.670	-0.668
	0.8	1.796	-	-0.132	-0.131	11.892	11.930	-1.406	-1.401
	0.9	2.542	0.981	-0.215	-	34.330	-	-4.891	-
4	0.1	0.987	1.006	-0.129	-0.128	1.209	1.199	-0.239	-0.237
	0.2	1.006	1.037	-0.127	-0.126	1.368	1.368	-0.251	-0.251
	0.3	1.038	1.086	-0.127	-0.126	1.653	1.655	-0.288	-0.288
	0.4	1.088	1.163	-0.130	-0.131	2.100	2.102	-0.359	-0.358
	0.5	1.161	1.273	-0.138	-0.136	2.805	2.806	-0.484	-0.483
	0.6	1.271	1.446	-0.151	-0.148	3.998	4.001	-0.716	-0.714
	0.7	1.445	1.752	-0.177	-0.175	6.284	6.298	-1.208	-1.204
	0.8	1.750	-	-0.229	-0.226	11.768	11.780	-2.532	-2.515
	0.9	2.457	0.962	-0.370	-	33.735	-	-8.797	-
10	0.1	0.968	0.987	-0.175	-0.172	1.229	1.222	-0.340	-0.336
	0.2	0.986	1.017	-0.172	-0.168	1.369	1.366	-0.349	-0.348
	0.3	1.018	1.065	-0.171	-0.171	1.648	1.648	-0.399	-0.394
	0.4	1.065	1.135	-0.174	-0.172	2.089	2.090	-0.495	-0.491
	0.5	1.135	1.239	-0.183	-0.181	2.787	2.789	-0.664	-0.661
	0.6	1.238	1.400	-0.199	-0.196	3.967	3.968	-0.979	-0.973
	0.7	1.400	1.685	-0.231	-0.226	6.224	6.227	-1.648	-1.634
	0.8	1.684	-	-0.295	-0.292	11.611	11.590	-3.450	-3.414
	0.9	2.338	0.943	-0.470	-	32.984	-	-11.968	-
100	0.1	0.946	0.964	-0.206	-0.207	1.252	1.251	-0.425	-0.424
	0.2	0.964	0.994	-0.202	-0.201	1.370	1.376	-0.429	-0.429
	0.3	0.995	1.039	-0.201	-0.198	1.642	1.647	-0.485	-0.470
	0.4	1.039	1.104	-0.203	-0.200	2.078	2.083	-0.598	-0.569
	0.5	1.105	1.202	-0.212	-0.208	2.770	2.772	-0.799	-0.793
	0.6	1.200	1.350	-0.229	-0.226	3.937	3.906	-1.173	-1.171
	0.7	1.350	1.611	-0.262	-0.257	6.165	6.157	-1.972	-1.957
	0.8	1.610	-	-0.329	-0.325	11.459	11.43	-4.121	-4.075
	0.9	2.210		-0.517	-	32.267	-	-14.277	-

Table 6 Normalized stress intensity factors $K_I / \sigma\sqrt{\pi a}$ of a single circumferential crack in a round bar

a/R	Penny-shaped crack			Circumferential surface crack		
	Axisy model	3-D model	Benthern and Koiter [25]	Axisy model	3-D model	Nisitani and Noda [26]
0.1	0.6369	0.6369	0.6369	1.181	1.183	1.180
0.2	0.6393	0.6394	0.6396	1.262	1.262	1.261
0.3	0.6462	0.6462	0.6468	1.393	1.393	1.393
0.4	0.6600	0.6600	0.6616	1.602	1.602	1.602
0.5	0.6855	0.6856	0.6881	1.939	1.939	1.940
0.6	0.7294	0.7294	0.7335	2.514	2.514	2.516
0.7	0.8067	0.8067	0.8123	3.615	3.615	3.618
0.8	0.9551	0.9552	0.9613	6.238	6.238	6.243
0.9	1.3218	1.3217	1.3251	16.66	16.66	16.67